

Stress accumulation and increased seismic risk in eastern Turkey

Suleyman S. Nalbant^{a,1,*}, John McCloskey^b, Sandy Steacy^b,
Aykut A. Barka^c

^a Geophysics Department, Istanbul University, Avcilar, Istanbul, Turkey

^b Geophysics Research Group, School of Environmental Studies, University of Ulster, Coleraine, Co., Derry, UK

^c Eurasian Earth Science Institute, Istanbul Technical University, Istanbul, Turkey

Received 10 September 2001; received in revised form 27 November 2001; accepted 27 November 2001

Abstract

Unlike the North Anatolian fault zone, which has produced 11 large earthquakes since 1939, the East Anatolian fault zone (EAFZ) has been relatively quiescent in the last century when compared to historical records and has therefore accumulated significant stresses along its length. Determination of the location and likely magnitude of a future probable earthquake along the EAFZ is of interest both because of this history of large earthquakes, ($M \approx 8$), and the density of population in the area. Here we calculate stress evolution along the fault zone due to both seismic and tectonic loading since 1822. A sequence of 10 well constrained historical earthquakes is selected and the resulting stresses are calculated, summed with tectonic loading stresses and resolved onto the mapped active faults. We identify two areas of particular seismic risk, one of which might be expected to yield a large event. Our results are sensitive to the previous history of large earthquakes in the region and indicate a need for detailed investigations to constrain the exact rupture geometries of previous earthquakes on these segments. © 2002 Elsevier Science B.V. All rights reserved.

Keywords: East Anatolian Fault; seismic risk; stress

1. Introduction

Many recent studies [1–6] have shown that earthquakes produce stress perturbations in the

crust which can significantly advance or retard events on neighbouring faults. It has become clear that the modelling of these co-seismic stress increases, together with the inter-seismic stress loading due to tectonic plate motions, can provide useful information on the state of stress on faults in a given region and can help in the elucidation of temporal variations of seismic hazard. Both Stein et al. [5] and Nalbant et al. [6], in 1997 and 1998 respectively, for example, identified the Izmit Bay area in western Turkey as being of particularly high risk. This area suffered a devastating magnitude $M_w = 7.4$ earthquake in 1999.

* Corresponding author. Tel.: +44-28-7032-4041;
Fax: +44-28-7032-4911.

E-mail address: ss.nalbant@ulst.ac.uk (S.S. Nalbant).

¹ Present address: Geophysics Research Group, School of Environmental Studies, University of Ulster, Coleraine, Co., Derry, UK.

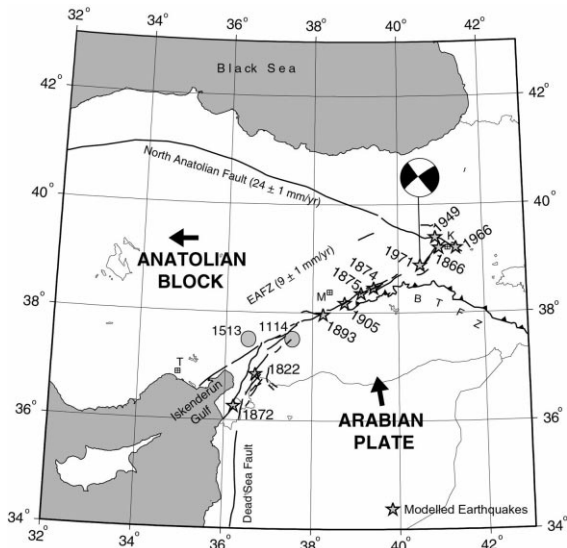


Fig. 1. Location map of earthquakes (stars) used for Coulomb modelling with the year of occurrence and the tectonic setting of eastern Anatolia as well as long-term slip rates of major faults. A typical focal mechanism solution for the zone is shown (after [8]). BTFZ, Bitlis thrust and folding zone. Also shown are the estimated epicentres of the 1114 and 1513 earthquakes (grey circles) after [9] and the cities of Tarsus (T) and Malatya (M) which are discussed in the text. Bold arrows indicate the relative movements of the plates.

Following this earthquake, Barka [7] noted increased loading on fault segments at either end of the rupture; the Bolu-Duzce segment failed 3 months later in an $M_w = 7.1$ event. Here we use the Coulomb stress modelling technique [1] to calculate stress evolution along the East Anatolian fault zone (EAFZ) due to both seismic and tectonic loading and try to identify regions that are significantly advanced toward failure.

The EAFZ forms a 580 km left-lateral strike-slip transform boundary between the northward moving Arabian Plate and westward moving Anatolian Block (Fig. 1). Translation rates of these plates are well constrained by global positioning system measurements throughout the region [10,11] and the 18–25 mm/yr northward movement of the Arabian Plate results in a 9 ± 1 mm/yr left-lateral movement along the EAFZ [11]. Since the beginning of the 19th century, all the large events in the area have been well recorded in both location and magnitude and correspond to mapped active faults [9,12,13] (Fig. 1). For ear-

lier earthquakes, however, it is generally impossible to ascertain either epicentres or magnitudes with confidence and we have, therefore, selected a sequence of 10 consecutive historical earthquakes, the first of which occurred in 1822, for our Coulomb modelling. The rupture parameters of these events are given in Table 1.

2. Materials and methods

To calculate stresses, we simulate faults as dislocation surfaces in an elastic half space and calculate stress perturbations due to slip on them using a three-dimensional (3D) boundary element technique [15]. A change in Coulomb stress ($\Delta\sigma_f$) is given by:

$$\Delta\sigma_f = \Delta\tau + \mu'\Delta\sigma_n \quad (1)$$

where $\Delta\tau$ and $\Delta\sigma_n$ are the changes in shear and normal stress on the fault planes of interest and μ' is the apparent friction coefficient. Although the average value of the coefficient of friction under laboratory conditions is generally between 0.6 and 0.8, it appears, based on aftershock distribution studies [16–18], that μ' can be as low as 0.0–0.3 in reality. This implies significant influence of fluids in real fault zones. Here we chose $\mu' = 0.4$ although our calculations are not sensitive to this value.

Since the actual geometry of active faults in the EAFZ is known, we digitise the active faults and resolve the 3D stress perturbation tensors resulting from previous earthquakes onto these digitised segments with full regard to their actual 3D orientations and slip directions in order to map Coulomb stress changes. The calculations were performed at a 2 km spacing along the segments at a depth of 6.5 km.

To include the effect of tectonic loading due to steady movement of the lower crust, we follow an approach used by many authors including [3,5,15]. The observed slip rate of 9 mm/yr [11] is applied to a boundary located at depths from 19 to 100 km vertically below the active faults. The slip is then tapered to 3 mm/yr at 13 km depth to reduce edge effects. This procedure yields

the stress increment per year due to tectonic loading for every fault segment. The inter-seismic Coulomb stress change per year is calculated at 6.5 km depth, which is approximately half the depth of the seismogenic layer, and multiplied by the number of years in the time period of interest; this change is then added to the co-seismic Coulomb stress change due to earthquakes in the same period. Each point on a given structure is coloured depending on its actual stress change including both the co-seismic and inter-seismic stress accumulation.

Note that in this paper we make no distinction between slow secular stress changes (approximately 0.056 bar/yr) and rapid co-seismic changes (often bars to 10s of bars). Although a number of authors (e.g. [19,20]) have argued that such co-seismic perturbations have a highly amplified effect on short-term earthquake probabilities, any such effects would be transient and hence not relevant at the time-scales considered here.

3. Results

Figs. 2 and 3 show the stress evolution along

the EAFZ since 1822; Fig. 2 contains series of snapshots while Fig. 3 illustrates the time history of the evolving stress. In each panel of Fig. 2, fault segments which have already failed are outlined with broken lines and those which have yet to fail are outlined with solid lines.

The Coulomb stress perturbation resulting from the 1822 and 1866 earthquakes is shown in Fig. 2a. Note that the 1822 event causes a stress increase ranging from 1.6 bar in the south to 2.1 bar in the north along the future 1872 fault segment. There is no significant seismic loading of the segments between Elazığ (E) and Bingöl (B) region (EB region) during this period. However, the 1822 event increased stress in the KM region between Kahraman Maras (K) and Malatya (M) by as much as 8 bar at its southern end. The 1866 events increased stress by more than 11 bar on the 1971 fault plane. This state of stress is represented by the black line in Fig. 3.

Fig. 2b shows the same scenario with the addition of tectonic loading for the interval 1822–1872. The 1971 segment gains an extra 2.9 bar of stress and the KM segment gains 2.7 bar. During the same time the EB segment accumulates a total of 3.4 bar (Fig. 3, purple curve).

Table 1
Modelled earthquakes ($M_s \geq 6.6$) on and around the EAFZ since 1822

No	Date	Epicentre (°)	Magnitude (M_s)	Fault Length (km)	Slip (cm)		Earthquake
					Strike ^a	Dip ^b	
1	1822, Aug. 13	36.7–39.9	7.5	140 ^c	500.0	0.0	Antakya
2	1866, May 12	39.2–41.0	7.2	45	424.0	0.0	
3	1872, Apr. 3	36.4–36.5	7.2	34	313.0	0.0	Amik Gölü
4	1874, May 3	38.5–39.5	7.1	45	177.0	200.0	Gölcük Gölü
5	1875, Mar. 27	38.5–39.5	6.7	20	181.0	0.0	
6	1893, Mar. 2	38.0–38.3	7.1	54	267.0	0.0	S. Malatya
7	1905, Dec. 4	38.1–38.6	6.8	38	252.0	0.0	
8	1949, Aug. 17	39.6–40.5	6.9	38	–178.0	0.0	Elmalidere
9	1966, Aug. 19	39.2–41.5	6.8	30	–160.0	0.0	Varto
10	1971, May 22	38.9–40.5	6.8	38	60.0	0.0	Bingöl

Epicentres, magnitudes and observed fault lengths are from [9,13]. In cases of lack of observation and information for fault length and slip values, empirical relations of [13], estimated for the Anatolian earthquakes, are used to calculate fault length (L /km), $\log(L) = -4.09 + 0.82M_s$ where M_s , surface wave magnitude. The moment (M_o in Nm) is then given by $\log(M_o) = 9.0 + 1.5M_s$ and the slip (u /m) is calculated by $u = M_o/(LWG)$ [14] where W is the down-dip width (km), and G is the shear modulus (here 3.0×10^{10} N/m²).

^a If the slip value is negative, the rupture is right-lateral, otherwise it is left-lateral.

^b If the dip slip value is negative, the movement is normal, otherwise it is thrust.

^c Although the fault length given in the literature [13] is 200 km, we here chose 140 km which is more consistent with both the known active faults in the area and with the empirical relationships given in [13].

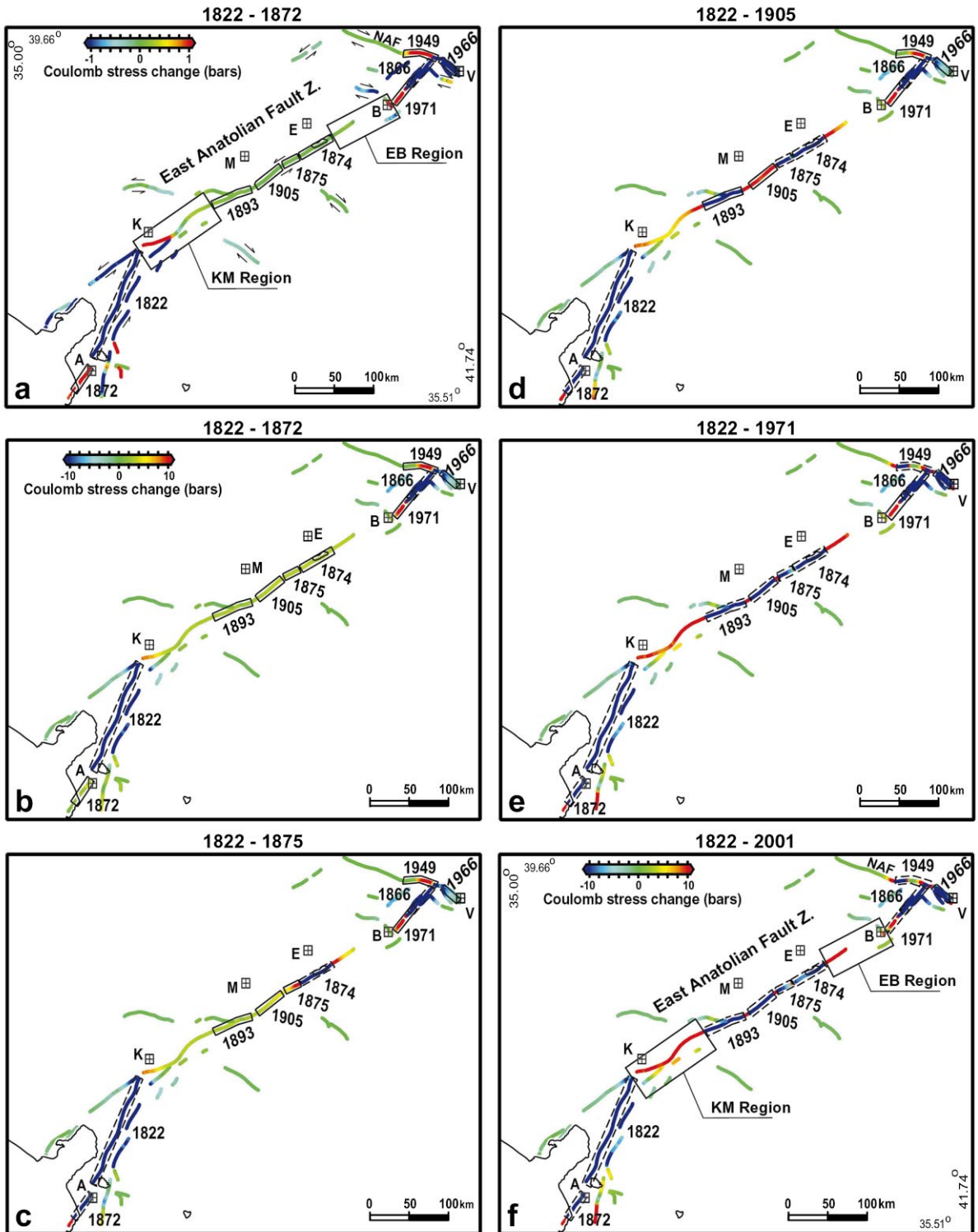


Fig. 2. Stress evolution along the EAFZ since 1822. In each panel, fault segments which have already failed are outlined with broken lines and those which have yet to fail are outlined with solid lines. The faults are thought to extend from the surface to 13 km depth, the average thickness of the seismogenic layer, and the stresses are calculated at a depth of 6.5 km. In (a) we show the seismic stress perturbation only whereas in all other figures we include both seismic and inter-seismic stress accumulation. With the exception of (a) all colour scales are the same. Arrows close to the faults show sense of relative movements. Large cities in the area are indicated by letters: A, Antakya; K, Kahraman Maras; M, Malatya; E, Elazig; B, Bingöl; and V, Varto. Two areas of particular interest (the KM and EB regions) are outlined with solid rectangles. (a) Stress resulting from earthquakes between 1822 and 1872. (b) As (a) but also including the tectonic loading for the 50 yr from 1822 to 1872. (c) The situation immediately before the 1875 event. (d) Total stress immediately before the 1905 earthquake. (e) Total stress accumulation prior to the 1971 event. (f) Total stress change from 1822 until the present. Stress levels on the KM segment range from 12.4 bar in the centre of the segment to >20 bar at the NE end. The stress levels on the EB segment range from 13.2 in the north to 16.3 near Elazig.

←

The stress state immediately before the 1875 event is shown in Figs. 2c and 3 (yellow curve). The stress load due to the secular movement has reached about 3 bar along the main branch of the EAFZ and the 1875 segment has accumulated up to 10 bar of stress. In addition, the north–east section of the 1905 fault has received about 0.8 bar of positive stress change from the 1874 event. Stress in the EB region has now increased by up to 7.8 bar since 1822. Note that despite the ab-

sence of significant loading from the sequence modelled here, the area north of the KM region failed in 1893.

Figs. 2d and 3 (blue curve) illustrate the stress situation immediately before the 1905 earthquake. Secular stress loading along the 1905 fault plane has reached about 5.8 bar. The 1893 earthquake has also transferred some 8.1 bar to the 1905 segment. The stress level in the KM region to the south–west of the 1893 earthquake has reached

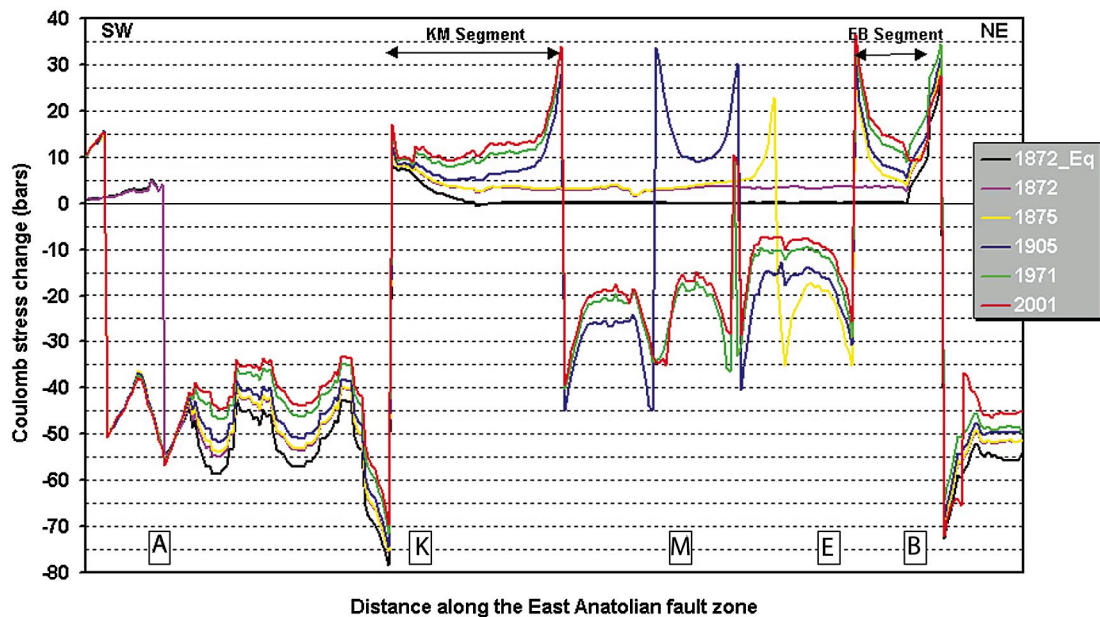


Fig. 3. Coulomb stress change history plots along the EAFZ during the study period (1822–2001). Each curve represents the stress state immediately prior to the earthquake that occurred in the labelled year. In order to reduce unrealistic edge effects, the stress values at the edges (five points) are smoothed. The capital letters are abbreviations for the cities in the region, same as in Fig. 2.

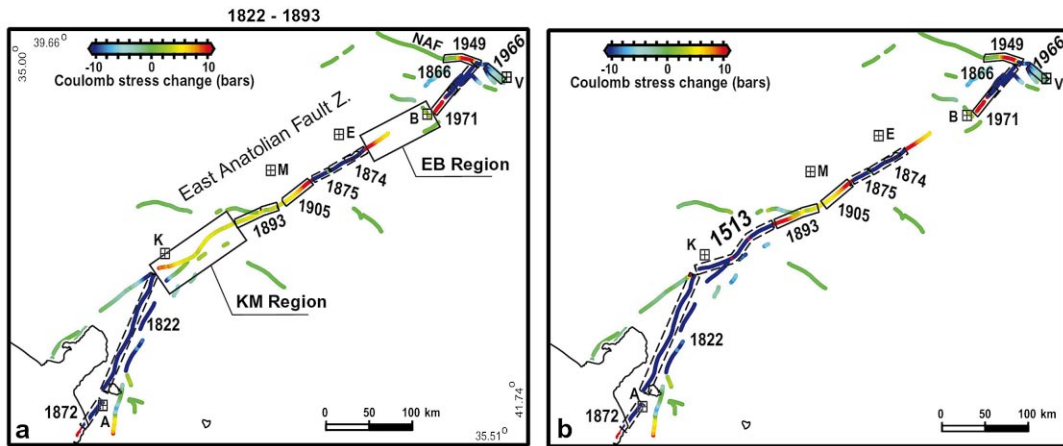


Fig. 4. (a) Stress on the EAFZ immediately prior to the 1893 earthquake assuming a 1822 baseline. Fault segments which have failed during the study period are outlined with broken lines and those which have failed subsequent to 1893 are outlined with solid lines. Note the low Coulomb stress (2–4 bar) along the length of the future 1893 rupture. (b) Stress on the EAFZ immediately prior to the 1893 earthquake assuming that an $M=7.4$ [13] 1513 earthquake ruptured 103 km of the fault zone in the KM region. Note that the Coulomb stress on the 1893 segment has increased to 20 bar at its SW tip; this stress change may explain the anomalously low calculated stress preceding the 1893 event.

17 bar and that to the south of the EB region has reached nearly 10 bar.

The total stress accumulation prior to the 1971 event is shown in Figs. 2e and 3 (green curve). Stresses during this period have reached about 18 bar in the region of the 1971 fault plane. Notice that the average stress in the KM region is now greater than 10 bar and is significantly higher at both ends due to the influence of the 1822 and 1893 earthquakes. The stress in the EB region has now reached a maximum of 13.8 bar near Elazig (E).

Figs. 2f and 3 (red curve) illustrate the present-day stress situations including both seismic and tectonic stress perturbations since 1822. Stress levels are generally low with two striking exceptions; Coulomb stress in the KM region now ranges from 12.4 bar in the centre of the area to >20 bar at the NE end while the stress levels in the EB region range from 13.2 in the north to 16.3 near Elazig. A rupture initiating in either area of high stress might be expected to propagate along the entire segment due to significant prior loading in the region and to dynamic stress concentrations which arise at rupture fronts overcoming locally strong (or under-stressed) patches on the fault [21].

4. Discussion

Our modelling unambiguously identifies two regions of the EAFZ which have been significantly loaded in the past 200 yr or so (Figs. 2f and 3) and which might produce the next large earthquake in the area. These are (a) the KM region, which extends between the cities of Kahraman Maras and Malatya and which has accumulated in excess of 20 bar of Coulomb stress locally, and (b) the EB region between the cities of Elazig and Bingöl which has accumulated over 15 bar during the study period. What are the seismic histories in these areas and what, if anything, can be inferred about the potential hazard?

Very little is known about previous activity on the EB region and, indeed, it is not clear whether it contains a through-going structure capable of producing a large earthquake. We cannot, therefore, infer anything about the seismic outlook here. The KM region, by contrast, is cut by a continuous fault segment which, were it to fail in one event, might produce a great earthquake ($M_w \geq 7.3$).

The KM region also has a history of large earthquakes that are consistent with having occurred on this fault segment. In 1114 a very large

earthquake occurred somewhere in the area whose magnitude is thought to be ≥ 7.8 [13]. Another large event occurred in 1513 and caused extensive damage in the cities of Tarsus and Malatya and is thought to have been felt as far away as Egypt [1]. Based on the distribution and intensity of damage it is believed to have been of a magnitude ≥ 7.4 [1]. These events, which are clearly important in the stressing history of the area, could not be included in our stress calculations since their locations and magnitudes are not sufficiently constrained. If, however, they did occur on the KM region they would have had a significant effect on our results. Indeed, some details of our results tend to support this possibility.

Colours representing stresses in Fig. 2 and the stress change curves in Fig. 3 assume that the crust was uniformly unstressed in 1822. This was clearly not the case and the EAFZ would have been subject to a strongly heterogeneous stress field at that time due to previous cycles of earthquake activity. The anomalously low stress increase (given the 1822 baseline) which activated the 1893 event (Fig. 4a) suggests that this area was already advanced towards failure prior to 1822. If we assume that the great earthquake of 1513 occurred on the KM region, assign a reasonable slip distribution to it and recalculate the stress on the 1893 segment, its stress is significantly increased (Fig. 4b) prior to failure and its anomalous occurrence is explained.

5. Conclusions

Our results show that, in the majority of cases, the order of events in the sequence can be explained by advance-to-failure due to stress interactions with preceding events. These results are consistent with earlier studies, most notably those on the North Anatolian fault zone [5,6]. Of more general interest, however, the stress modelling presented in this paper clearly indicates a build-up of stress in the KM region of the EAFZ. This fact together with the history of large earthquakes whose locations are consistent with activity on the KM region, force us to conclude then that: firstly, the KM region is the most likely location of the

next damaging earthquake on the EAFZ and, secondly, it is likely to produce a very large ($M_w \geq 7.3$) event.

If these conclusions are to be further substantiated, it is imperative that we obtain more detailed information on the history of seismicity on the KM region. Previous great events here would almost certainly have produced surface ruptures which might be exposed by palaeoseismology in which active faults are excavated by trenching and ancient ruptures dated using radiometric techniques [22]. We, therefore, strongly recommend that a detailed palaeoseismological investigation should be carried out as a matter of urgency with the aims of location and quantification of the precise geometry of the 1114 and 1513 ruptures.

Acknowledgements

We greatly appreciate constructive reviews of Ruth A. Harris and Ross Stein. We thank L. Sykes and C. Scholz for their suggestions at the initial stage of this study while one of the authors (S.S.N.) was visiting the Lamont-Doherty Earth Observatory of Columbia University. We would also like to thank Sally Cook, Rachel Cassidy and Rosemarie McMenamin for reading an earlier version of the paper. This study was supported by Istanbul University Research fund, project no. 1047/031297, and by a NATO-TUBITAK (B-2) post-doctoral fellowship. The study also benefited from an EC funded project, Towards Practical, Real-Time Estimation of Spatial After-shock Probabilities: a Feasibility Study in Earthquake Hazard (PRESAP). [RV]

References

- [1] R.S. Stein, G.C.P. King, J. Lin, Change in failure stress on the southern San Andreas fault system caused by the 1992 Magnitude=7.4 Landers earthquake, *Science* 258 (1992) 1328–1332.
- [2] R.A. Harris, R.W. Simpson, Changes in static stress on southern California faults after the 1992 Landers earthquake, *Nature* 360 (1992) 251–254.
- [3] R.W. Simpson, P.A. Reasenber, Earthquake-induced

- static stress changes on central California faults, in: R.W. Simpson (Ed.), *The Loma Prieta, California Earthquake of October 17, 1989—Tectonic Processes and Models*, U.S. Geological Survey Prof. Paper 1550-F, 1994, F55–F89.
- [4] S.C. Jaumé, L.R. Sykes, Evolution of moderate seismicity in the San Francisco Bay region, 1850 to 1993: Seismicity changes related to the occurrence of large and great earthquakes, *J. Geophys. Res.* 101 (1996) 765–789.
- [5] R.S. Stein, A.A. Barka, J.H. Dieterich, Progressive failure on the North Anatolian fault since 1939 by earthquake stress triggering, *Geophys. J. Int.* 128 (1997) 594–604.
- [6] S.S. Nalbant, A. Hubert, G.C.P. King, Stress coupling between earthquakes in northwest Turkey and the north Aegean Sea, *J. Geophys. Res.* 103 (1998) 24469–24486.
- [7] A. Barka, The 17 August 1999 Izmit earthquake, *Science* 285 (1999) 1858–1859.
- [8] T. Taymaz, H. Eyidogan, I. Kucsu, Source parameters of large earthquakes in the East Anatolian fault zone (Turkey), *Geophys. J. Int.* 106 (1992) 537–550.
- [9] N. Ambraseys, Temporary seismic quiescence in SE Turkey, *Geophys. J.* 96 (1989) 311–331.
- [10] R.E. Reilinger et al., Global positioning system measurements of the present-day crustal movements in the Arabia–Africa–Eurasia plate collision zone, *J. Geophys. Res.* 102 (1997) 9983–9999.
- [11] S. McClusky et al., Global positioning system constraints on plate kinematics and dynamics in the eastern Mediterranean and Caucasus, *J. Geophys. Res.* 105 (2000) 5695–5719.
- [12] N.N. Ambraseys, C.P. Melville, Historical evidence of faulting in Eastern Anatolia and Northern Syria, *Ann. Geofis.* 38 (1995) 337–344.
- [13] N. Ambraseys, J.A. Jackson, Faulting associated with historical and recent earthquakes in the Eastern Mediterranean region, *Geophys. J. Int.* 133 (1998) 390–406.
- [14] H. Kanamori, D.L. Anderson, Theoretical basis of some empirical relations in seismology, *Bull. Seism. Soc. Am.* 65 (1975) 1073–1095.
- [15] J. Gomberg, M.A. Ellis, Topography and tectonics of the New Madrid seismic zone: Results of numerical experiments using a three-dimensional boundary element program, *J. Geophys. Res.* 99 (1994) 20299–20310.
- [16] Y.Y. Kagan, D.D. Jackson, Spatial aftershock distribution: Effect of normal stress, *J. Geophys. Res.* 103 (1998) 24453–24467.
- [17] S. Gross, R. Burgmann, The rate and state of background stress estimated from aftershocks of the 1989 Loma Prieta, California, earthquake, *J. Geophys. Res.* 103 (1998) 4915–4927.
- [18] P.A. Reasenberg, R.W. Simpson, Response of regional seismicity to the static stress change produced by the Loma Prieta earthquake, *Science* 255 (1992) 1687–1690.
- [19] J.H. Dieterich, B. Kilgore, Implications of fault constitutive properties for earthquake prediction, *Proc. Natl. Acad. Sci. USA* 93 (1996) 3787–3794.
- [20] S. Toda, R.S. Stein, P.A. Reasenberg, J.H. Dieterich, Stress transferred by the Mw = 6.5 Kobe, Japan, shock: Effect on aftershocks and future earthquake probabilities, *J. Geophys. Res.* 103 (1998) 24543–24565.
- [21] S.J. Steacy, J. McCloskey, What controls an Earthquake's size? Results from a heterogeneous cellular automation, *Geophys. J. Int.* 133 (1998) f11–f14.
- [22] K. Sieh, M. Stuiver, D.A. Brillinger, More precise chronology of earthquakes produced by the San Andreas fault in southern California, *J. Geophys. Res.* 94 (1989) 603–623.